Beyond blood ammonia: Intestinal ammonia emerges as an early microbial driver of mild cognitive impairment

Hao Chen[1, #], Zhen Wang[1, #], Yajun Tang[1], Yahui Liu[1], Lihui Kou[1], Jing Huang[2, *], Ke Guo[3, *], Zheng Yu[1, *]

[1]Human Microbiome and Health Group, Department of Microbiology, Xiangya School of Basic Medical Sciences, Central South University, Changsha, Hunan 410001, China

[2]Human Microbiome and Health Group, Department of Parasitology, Xiangya School of Basic Medical Sciences, Central South University, Changsha, Hunan 410001, China

[3]Department of Neurology, Third Xiangya Hospital, Central South University, Changsha, Hunan, 410001, China

*** Correspondence authors:** Zheng Yu, yuzheng@csu.edu.cn; Ke Guo, guokexy3yy@csu.edu.cn; Jing Huang jing_huang@csu.edu.cn

[#] These authors contributed equally.

Abstract: Mild cognitive impairment (MCI) is an early and potentially reversible stage of neurodegenerative disease, yet its initiating pathogenic signal remains unclear. Here, we identify gut microbiota-derived, urease-dependent intestinal ammonia as an early functional contributor to cognitive impairment. Analyses of human MCI-related cohorts revealed increased fecal urease activity and ammonia-related microbial features associated with cognitive performance. Importantly, intestinal ammonia accumulation precedes detectable elevations in blood ammonia, indicating that local intestinal dysregulation occurs before systemic hyperammonemia. Mechanistically, ammonia suppresses colonic SMAD7 and activates JAK2 signaling in the brain, thereby promoting cognitive dysfunction independently of systemic ammonia toxicity. This signaling pattern was further supported in 5xFAD mice. Therapeutically, supplementation with the ammonia-assimilating bacterium *Limosilactobacillus mucosae* or treatment with the clinically used ammonia-lowering agent L-ornithine-L-aspartate reduces intestinal ammonia levels and ameliorates early cognitive deficits. Together, these findings define an ammonia-SMAD7-JAK2 axis linking gut metabolism to brain function and highlight intestinal ammonia as a promising therapeutic target for early cognitive impairment.

Keywords: intestinal ammonia, microbial urease, mild cognitive impairment, cognitive decline, SMAD7-JAK2 signaling

Significance statement

Mild cognitive impairment is an early, potentially reversible stage of neurodegenerative disease, yet its initiating biological signals remain poorly defined. This study reveals that ammonia produced by gut microbial urease acts as an early driver of cognitive decline before blood ammonia levels rise. Elevated intestinal ammonia was associated with cognitive impairment-like phenotypes, accompanied by reduced colonic SMAD7 and increased brain JAK2 in experimental models. Bacterial and pharmacological interventions lowered intestinal ammonia and improved cognitive performance in these models. These findings redefine ammonia as a gut-brain signaling metabolite and identify intestinal ammonia metabolism as a promising target for early diagnosis and intervention in cognitive impairment.

Background

Mild cognitive impairment (MCI) represents a central and early feature of many neurodegenerative diseases, including Alzheimer's disease (AD) and Parkinson's disease [1]. These disorders are characterized not only by progressive loss of cognitive abilities but also by underlying pathological changes such as synaptic dysfunction, neuronal loss, and neuroinflammation [2]. For instance, in AD, cognitive decline closely correlates with hallmark amyloid-β plaques and tau tangles in the brain, and the progression from MCI to overt dementia has been well documented in aging populations [3]. Beyond classical neuropathology, cognitive dysfunction also involves dysregulation of neural circuits responsible for learning, memory, and executive processes, significantly impairing quality of life and imposing an increasing health burden with global population aging [4]. Despite extensive research, effective strategies to prevent or reverse neurodegenerative cognitive decline remain limited, highlighting the need to elucidate novel mechanisms underlying early cognitive deficits.

Emerging evidence indicates that the gut microbiome plays a critical role in regulating brain function and cognitive health. The gut-brain axis constitutes a bidirectional communication network involving neural, immune, endocrine, and metabolic pathways [5]. Among various microbial metabolites, ammonia has attracted attention due to its neuroactive properties. Elevated systemic or cerebral ammonia, as observed in conditions such as hepatic encephalopathy, can impair astrocyte function, trigger neuroinflammation, disrupt neurotransmission, and ultimately contribute to cognitive deficits, highlighting the potential importance of gut-derived ammonia in neurodegenerative disease [6]. In the gut, microbial urease is the primary enzyme responsible for ammonia production, catalyzing the hydrolysis of urea into ammonia and carbon dioxide, and representing a key pathway through which gut bacteria regulate host nitrogen metabolism [7]. Although few studies have directly examined microbial urease in relation to cognitive impairment, recent evidence shows that ammonia, a product of bacterial urease activity, can modulate host neural metabolism and behavior, and that engineering the gut microbiota to reduce urease activity can mitigate ammonia-associated neurotoxicity [8, 9]. These findings suggest that targeting urease-producing bacteria may represent a mechanistic axis linking gut microbial activity to host cognitive outcomes.

Despite these advances, the mechanisms by which gut microbial urease-derived ammonia contributes to the pathogenesis of MCI remain largely unexplored. In particular, it is unclear whether intestinal ammonia functions as an early pathogenic mediator before systemic hyperammonemia develops, and whether its effects on cognitive performance are transmitted through local gut-brain signaling pathways independent of overt blood ammonia changes. Here, we aimed to delineate the role of gut microbiota-derived, urease-dependent ammonia in driving MCI progression and to uncover the underlying molecular pathways. By integrating fecal metagenomic analyses from public MCI-related cohorts and an independent clinical MCI cohort, we observed ammonia metabolism-related microbial alterations associated with cognitive impairment. We then used a 5-FU-induced chemotherapy-associated MCI-like model to examine the temporal sequence and functional contribution of intestinal ammonia dysregulation, and further used 5xFAD mice to evaluate whether this pathway is also present in an AD-relevant genetic model. Together, these analyses support a convergent model in which distinct cognitive impairment contexts may exhibit partially overlapping intestinal ammonia-related metabolic alterations accompanied by SMAD7-JAK2 signaling changes. These results identify intestinal ammonia as an early, causally relevant, and actionable driver of

MCI, highlighting microbial ammonia suppression as a potential therapeutic strategy to delay disease progression.

Results

Gut microbiota-derived urease activity drives early intestinal ammonia accumulation during cognitive impairment

To determine whether cognitive impairment is accompanied by alterations in gut microbiota-derived ammonia metabolism, we first analyzed fecal metagenomic data from a public MCI-related cohort and further examined ammonia-related readouts in an independent clinical cohort (**Figure 1A**). The independent clinical cohort included 20 healthy controls and 28 patients with clinically diagnosed MCI. To characterize potential demographic and clinical confounders, we compared baseline characteristics between the two groups. No statistically significant differences were observed in age, sex distribution, diabetes, hypertension, coronary heart disease, or dyslipidemia, whereas both Mini-Mental State Examination (MMSE) and Montreal Cognitive Assessment (MoCA) scores were significantly lower in the MCI group, consistent with the presence of cognitive impairment **(Supplementary Figure 1)**. Because not all individuals with MCI necessarily represent prodromal Alzheimer's disease, we further assessed AD-related biomarker and genetic-risk features in available samples. Plasma amyloid-β 42 (Aβ42) levels were significantly increased in the MCI group compared with healthy controls **(Supplementary Figure 2A)**. Apolipoprotein E (APOE) genotyping further showed that both APOE ε4 carrier frequency and ε4 allele frequency were higher in the MCI group than in healthy controls **(Supplementary Figure 2B** and **2C)**. These findings suggest that the clinical MCI cohort carries a higher burden of AD-related risk features and may include individuals with increased susceptibility to AD-related cognitive decline. However, because longitudinal follow-up and comprehensive AD biomarker confirmation were not available, we cannot determine whether these individuals will progress to AD. Metagenomic analysis revealed a significant enrichment of key urease-encoding genes (*ureA*, *ureB*, and *ureC*) in the public MCI cohort, a trend that was consistently observed in the clinical cohort (**Figure 1B, 1C**). Accordingly, the predicted overall abundance of urease was markedly increased in individuals with MCI, suggesting that urease-dependent intestinal ammonia-producing capacity is activated at an early stage of disease (**Figure 1D**). To directly assess whether these genomic alterations translate into functional enhancement of ammonia metabolism, we quantified fecal urease activity and ammonia levels in the clinical MCI cohort. Both fecal urease activity and ammonia levels were significantly elevated in MCI patients and exhibited a strong negative correlation with MMSE scores (**Figure 1E-1H**), indicating that enhanced intestinal ammonia production and local ammonia accumulation are closely associated with cognitive impairment severity.

To delineate the temporal sequence and potential contribution of intestinal ammonia dysregulation during cognitive impairment, we established a 5-fluorouracil (5-FU)-induced MCI-like mouse model (**Figure 1I**). The 5-FU-induced model was selected as a reproducible and experimentally tractable model of chemotherapy-associated cognitive impairment, enabling longitudinal assessment of intestinal microbial and metabolic alterations during the early development of cognitive impairment-like phenotypes. Fecal metagenomic analysis demonstrated a significant enrichment of urease-related genes and a marked increase in predicted urease abundance following 5-FU-induced MCI-like modeling (**Figure 1J, 1K**). Longitudinal monitoring revealed that intestinal

ammonia levels increased as early as day 2 after 5-FU-induced MCI-like modeling and remained persistently elevated, whereas blood ammonia levels showed no significant changes throughout the disease course (**Figure 1L, 1M**). Given that 5-FU can cause intestinal mucosal injury depending on the dose and treatment schedule, we used a relatively low-dose and low-frequency regimen and performed histological assessment of intestinal tissues. Hematoxylin and Eosin (H&E) staining showed no overt epithelial disruption or severe mucosal damage under this regimen, suggesting that the observed intestinal ammonia changes were unlikely to be simply secondary to gross mucosal injury **(Supplementary Figure 3A)**. These findings indicate that microbiota-derived intestinal ammonia accumulation represents an early pathological event during 5-FU-induced MCI-like progression and occurs independently of systemic hyperammonemia. Because this model was induced by 5-FU, we further analyzed a paired public fecal metagenomic cohort before and after 5-FU treatment to determine whether 5-FU exposure itself was associated with increased microbial ammonia-producing potential. No consistent increase in urease-related or ammonia-producing genes was observed after 5-FU treatment, suggesting that the urease-ammonia phenotype observed in 5-FU-induced MCI-like mice is unlikely to represent an inevitable direct consequence of 5-FU exposure alone **(Supplementary Figure 3B-3D)**. To further evaluate whether urease-dependent ammonia production functionally contributed to the MCI-like phenotype, we treated 5-FU-induced MCI mice with flurofamide (FFA), a bacterial urease inhibitor. FFA treatment significantly reduced intestinal ammonia levels in MCI mice and improved cognitive performance, including spontaneous alternation in the Y-maze, novel object recognition, and Morris water maze performance **(Supplementary Figure 3E-3J)**. These results indicate that urease-dependent intestinal ammonia production contributes to the cognitive impairment. We further examined whether intestinal ammonia dysregulation also occurs in an AD-relevant genetic model. At an early disease stage, 5xFAD mice showed increased intestinal ammonia levels compared with wild-type (WT) controls, indicating that early intestinal ammonia accumulation is not restricted to the 5-FU-induced chemotherapy-associated model. These data provide bridging evidence linking the AD-related metagenomic observations with the intestinal ammonia phenotype observed in experimental MCI-like models **(Supplementary Figure 3K)**.

To assess whether cohousing transfers ammonia-associated changes and behavioral phenotypes, we performed cohousing experiments between WT and MCI mice (**Figure 1N**). Cohousing significantly increased intestinal ammonia levels in WT mice while concomitantly reducing intestinal ammonia levels in MCI mice (**Figure 1O**). Behavioral assessments revealed that cohoused WT mice exhibited reduced exploratory behavior toward novel objects and impaired exploration of new environments (**Figure 1P-1S**). Consistently, Morris water maze testing demonstrated significantly impaired learning ability and spatial memory in cohoused WT mice (**Figure 1T, 1U**). Because cohousing transfers the entire gut microbial community rather than ammonia alone, we further tested whether urease-dependent ammonia production was required for the transferred phenotype. Treatment with the bacterial urease inhibitor FFA significantly reduced intestinal ammonia levels in cohoused WT mice and rescued MCI-like behavioral deficits, including spontaneous alternation, novel object recognition, learning performance, and platform-crossing frequency **(Supplementary Figure 4)**. These findings indicate that MCI-associated microbiota can transmit cognitive impairment-related phenotypes to WT mice and that this effect is largely dependent on urease-mediated intestinal ammonia production.

Urease-positive bacterial isolates drive MCI-like cognitive phenotypes via urease-mediated ammonia production

To identify key microbial taxa responsible for enhanced intestinal ammonia production during 5-FU-induced MCI-like progression, we systematically analyzed the relative contribution of different taxonomic groups to urease gene abundance. Following MCI onset, the relative contribution of Lactobacillales and Bifidobacteriales to total urease content decreased, whereas Enterobacterales and Pseudomonadales exhibited markedly increased contributions, indicating a disease-associated restructuring toward ammonia-producing bacterial communities (**Figure 2A**). Based on these findings, we isolated urease-positive bacterial strains from human fecal samples using a selective medium containing urea as the sole nitrogen source (**Figure 2B**). Taxonomic characterization revealed that most urease-positive isolates belonged to the orders Bacillales and Enterobacterales (**Figure 2C**). Examination of their abundance in mouse fecal metagenomes identified *Enterococcus faecium*, *Klebsiella oxytoca*, and *Pseudomonas fortuita* as the most dynamically altered species during 5-FU-induced MCI-like progression (**Figure 2D**). These three strains were therefore selected for oral administration to WT mice to evaluate their cognitive impact. Administration of all three ammonia-producing strains significantly increased intestinal ammonia levels in WT mice, with *P. fortuita* exerting the most pronounced effect, while blood ammonia levels remained unchanged (**Figure 2E, 2F**). Integration of behavioral outcomes using Z-score normalization revealed that *P. fortuita*-treated mice exhibited the lowest cumulative cognitive scores, indicating the strongest induction of MCI-like cognitive deficits (**Figure 2G, Supplementary Figure 5A-5D**). To determine whether the effect of *P. fortuita* was associated with urease-mediated ammonia production, we first validated the effect of FFA, a bacterial urease inhibitor, in vitro. *P. fortuita* was cultured with or without FFA, and medium without bacteria served as the blank control. FFA treatment markedly attenuated *P. fortuita* growth and significantly reduced ammonia accumulation and urease activity in the culture supernatant **(Supplementary Figure 5E-5G)**. We next administered FFA to *P. fortuita*-treated WT mice to evaluate the functional contribution of urease-mediated ammonia production in vivo (**Figure 2H**). FFA treatment significantly reduced intestinal ammonia levels **(Figure 2I)** and markedly improved cognitive performance, including enhanced exploration of novel objects and environments as well as improved spatial learning and memory (**Figure 2J-2M**). Fecal qPCR showed that FFA treatment significantly reduced both *P. fortuita* abundance and the abundance of the *P. fortuita*-derived *ureA* gene **(Supplementary Figure 5H)**. These findings indicate that FFA decreased the overall *P. fortuita*-associated urease burden in the gut. To obtain complementary evidence for a contribution of bacterial urease, we administered a recombinant *Escherichia coli* BL21 strain heterologously expressing urease to WT mice, with BL21 carrying an empty vector serving as control (**Figure 2N**). The urease-expressing strain significantly increased intestinal ammonia levels and exacerbated MCI-like cognitive deficits in WT mice (**Figure 2O-2S**), supporting that bacterial urease-driven ammonia production is sufficient to induce cognitive impairment-like phenotypes in mice. Together, these findings indicate that urease-positive bacteria, particularly *P. fortuita*, were accompanied by increased intestinal ammonia.

Intestinal ammonia contributes to MCI-like pathology through colonic SMAD7 suppression and brain JAK2 activation

To determine whether ammonia functions as a direct signaling molecule in MCI-associated pathology, WT mice were administered exogenous NH_4Cl (**Figure 3A**). NH_4Cl treatment

significantly elevated intestinal ammonia levels without affecting blood ammonia concentrations (**Figure 3B** and **3C**). Behavioral analyses revealed that ammonia-treated WT mice developed pronounced MCI-like cognitive deficits, including impaired performance in the Y-maze, novel object recognition, and Morris water maze tests (**Figure 3D-3G**). These results further support the notion that elevated intestinal ammonia can induce cognitive impairment-like phenotypes in the absence of systemic hyperammonemia. Given the observation that intestinal ammonia increases early during MCI while blood ammonia remains stable, we hypothesized that gut-derived ammonia influences brain function through colonic signaling pathways. To identify ammonia-responsive molecular pathways, we performed transcriptomic profiling of colon and brain tissues from NH_4Cl-treated mice. Non-metric multidimensional scaling (NMDS) analysis demonstrated significant shifts in both colonic and brain transcriptomes following NH_4Cl treatment, closely resembling those observed in MCI mice **(Supplementary Figure 6A)**. Gene set enrichment analysis (GSEA) revealed that the Th17 cell differentiation pathway was the most significantly enriched pathway associated with cognitive impairment in the brain, whereas the TGF-β signaling pathway emerged as the most relevant pathway in the colon (**Figure 3H** and **3I**). Within these pathways, *Smad7* in the colon and *Jak2* in the brain were identified as core genes most strongly associated with cognitive impairment. Notably, SMAD7 expression was significantly downregulated, while JAK2 expression was markedly upregulated, with highly consistent trends observed in both NH_4Cl-treated and MCI model mice (**Figure 3J**).

To validate the regulatory effects of ammonia on SMAD7 and JAK2 expression, dose-response experiments were conducted using NH_4Cl treatment. Exposure to 4 mM NH_4Cl significantly reduced SMAD7 expression while markedly increasing JAK2 expression, suggesting that ammonia may regulate this signaling axis through suppression of SMAD7 **(Supplementary Figure 6B)**. To determine whether SMAD7 negatively regulates JAK2, HEK293FT cells were transfected with Flag-SMAD7, and JAK2 protein levels were assessed by immunoblotting. Compared with empty vector controls, SMAD7 overexpression significantly reduced JAK2 protein abundance **(Supplementary Figure 6C)**. Consistently, co-transfection of Flag-SMAD7 and HA-JAK2 resulted in markedly lower JAK2 protein levels compared with HA-JAK2 transfection alone, further supporting a negative regulatory role of SMAD7 on JAK2 at the protein level **(Supplementary Figure 6D)**. In addition, immunofluorescence localization and intensity measurements in NIH3T3-L1 cells revealed that NH_4Cldecreased SMAD7 localization intensity, confirming that SMAD7 responds to NH_4Clintervention **(Supplementary Figure 6E)**. Moreover, enforced overexpression of SMAD7 markedly suppressed JAK2 expression, indicating that SMAD7 acts as a negative regulator of JAK2 **(Supplementary Figure 6F)**. To validate whether intestinal epithelial SMAD7 directly responds to ammonia exposure, immortalized mouse colonic mucosal epithelial cells (IMCCs) and Caco-2 cells were treated with different concentrations of NH_4Cl. NH_4Cl treatment reduced SMAD7 expression in a dose-dependent manner, indicating that ammonia can suppress SMAD7 in intestinal epithelial cells **(Figure 3K, Supplementary Figure 6G)**. To further examine whether epithelial SMAD7 can influence JAK2 signaling in brain-related cells, we established a Transwell co-culture system consisting of IMCCs in the upper chamber and C8-D1A astrocytes in the lower chamber **(Figure 3L)**. SMAD7 was overexpressed in the upper IMCCs compartment, and JAK2 expression was then examined in the lower astrocyte compartment. Overexpression of SMAD7 in IMCCs markedly reduced JAK2 protein levels in C8-D1A astrocytes, supporting a functional IMCCs SMAD7-astrocytic JAK2 regulatory relationship across the co-culture system

(Figure 3M).

To assess the in vivo relevance of intestinal ammonia-induced JAK2 activation, brain tissues from NH_4Cl-treated and MCI model mice were analyzed by immunoblotting. Both groups exhibited significantly elevated JAK2 protein levels compared with WT controls, indicating that increased intestinal ammonia may promote MCI-associated cognitive dysfunction through activation of brain JAK2 signaling (**Figure 3N**).These findings demonstrate that ammonia drives MCI-like cognitive impairment by suppressing colonic SMAD7 and activating the SMAD7-JAK2 signaling axis in the absence of systemic hyperammonemia. To functionally validate the contribution of colonic SMAD7 suppression to brain JAK2 activation and cognitive impairment, we performed an AAV-mediated SMAD7 rescue experiment in MCI mice. After establishment of the 5-FU-induced MCI-like model, AAV-SMAD7 or the corresponding control AAV vector was delivered by rectal enema to restore colonic SMAD7 expression (**Figure 3O**). Western blot analysis confirmed that AAV-SMAD7 increased SMAD7 expression in colonic tissues (**Figure 3P**). Functionally, AAV-SMAD7 treatment significantly improved MCI-like behavioral deficits, including spontaneous alternation in the Y-maze, novel object recognition, and Morris water maze performance (**Figure 3Q-3T**). Importantly, restoration of colonic SMAD7 was accompanied by reduced brain JAK2 protein levels (**Figure 3P**). To further determine whether this signaling pattern is also present in an AD-relevant genetic model, we analyzed colonic and brain tissues from 5xFAD mice. Consistent with the results from NH_4Cl-treated and 5-FU-induced MCI-like mice, 5xFAD mice exhibited decreased colonic SMAD7 expression and increased brain JAK2 protein levels **(Supplementary Figure 6G)**.

Collectively, these findings support a model in which intestinal ammonia contributes to MCI-like cognitive impairment by suppressing colonic SMAD7 and activating brain JAK2 signaling in the absence of systemic hyperammonemia.

L. mucosae mitigates MCI-like cognitive deficits by lowering intestinal ammonia levels

To evaluate whether targeted reduction of intestinal ammonia can attenuate MCI progression, we explored multiple ammonia-lowering strategies. Source tracking analysis revealed that the contribution of Lactobacillales to bacterial urease content was significantly reduced following MCI onset (**Figure 4A**). We next curated ammonia assimilation-related genes from the KEGG database and screened those annotated to *Lactobacillales* (**Figure 4B**). Five key ammonia assimilation genes were identified within Lactobacillales, all of which exhibited decreased abundance following MCI development (**Figure 4B**). Consistently, the overall abundance of *Lactobacillales* was significantly reduced in MCI mice (**Figure 4C**). These findings suggest that MCI is associated with a loss of *Lactobacillales*-derived ammonia assimilation potential, which may contribute to intestinal ammonia accumulation.

Based on these observations, *L. mucosae* was selected from an in-house bacterial library for intervention in MCI mice (**Figure 4D**). Administration of *L. mucosae* significantly reduced intestinal ammonia levels in MCI mice, restoring them to levels comparable to WT controls (**Figure 4E**). Behavioral analyses further demonstrated that live *L. mucosae* markedly ameliorated MCI-like cognitive deficits, including improved spontaneous alternation, novel object recognition, and Morris water maze performance (**Figure 4F-4I**). Moreover, *L. mucosae* significantly increased SMAD7 protein levels and decreased JAK2 protein levels, suggesting that ammonia reduction by *L. mucosae* may attenuate activation of the ammonia-associated JAK2 pathway (**Figure 4J**). To strengthen the

strain-specific interpretation of the *L. mucosae* intervention, we included two additional controls. Heat-killed *L. mucosae* was used to determine whether the effect required viable bacterial metabolism rather than bacterial structural components, whereas live Limosilactobacillus fermentum was included as a Lactobacillus control strain to assess whether the observed benefit simply reflected nonspecific restoration of commensal bacteria after antibiotic depletion. In vitro, live *L. mucosae*, heat-killed *L. mucosae*, and live *L. fermentum* were incubated in medium containing 5 mM NH_4Cl and glucose for 24 h. Live *L. mucosae* markedly reduced supernatant NH_4^+ levels compared with the blank control, whereas heat-killed *L. mucosae* and live *L. fermentum* showed significantly weaker ammonia-lowering effects **(Supplementary Figure 7A** and **7B)**. These results indicate that the ammonia-lowering capacity of *L. mucosae* depends on viable bacterial metabolism and is not simply a general Lactobacillus-associated effect. To further distinguish the protective effect of *L. mucosae* from nonspecific bacterial reconstitution after antibiotic treatment, we compared live *L. mucosae* with heat-killed *L. mucosae* and live *L. fermentum* in MCI mice under the same experimental conditions **(Figure 4K)**. Live *L. mucosae* significantly reduced fecal ammonia levels and improved MCI-like behavioral deficits, whereas heat-killed *L. mucosae* and live *L. fermentum* failed to reproduce the full ammonia-lowering and behavioral benefits observed with live *L. mucosae* **(Figure 4L-4P)**. These findings support a live, strain-preferential ammonia-lowering effect of *L. mucosae* rather than a nonspecific effect caused by the restoration of commensal bacteria after antibiotic depletion.

We next asked whether the ammonia-lowering effect of *L. mucosae* could also be extended to an AD-relevant genetic model **(Figure 4Q)**. In 5xFAD mice, *L. mucosae* intervention reduced intestinal ammonia levels and improved behavioral performance **(Figure 4R-4V)**. In parallel, western blot analysis showed restoration of colonic SMAD7 expression and reduction of brain JAK2 protein levels after *L. mucosae* treatment **(Figure 4W)**. These results indicate that the intestinal ammonia-SMAD7-JAK2 axis is not limited to the 5-FU-induced MCI-like model, but is also modifiable by *L. mucosae* intervention in an AD-related genetic model.

In addition, pharmacological intervention with the clinically approved ammonia-lowering agent L-ornithine L-aspartate (LOLA) was applied to NH_4Cl-treated mice **(Supplementary Figure 7C)**. LOLA treatment significantly reduced intestinal ammonia levels and effectively lowered blood ammonia concentrations, while simultaneously rescuing MCI-like functional impairments **(Supplementary Figure 7D-7I)**. Taken together, these findings consistently demonstrate that targeted reduction of intestinal ammonia represents a promising disease-modifying strategy for early-stage MCI prior to the onset of systemic hyperammonemia.

Discussion

For a long time, research on ammonia in neurological disorders has been predominantly framed around its neurotoxic properties [10, 11]. In particular, under conditions of systemic hyperammonemia such as hepatic encephalopathy, elevated blood ammonia has been widely regarded as a prerequisite for ammonia-induced central nervous system injury, while the intestine has largely been positioned as a site of ammonia production and release rather than an active node for signal integration and regulation [11, 12]. Our study substantially extends this traditional conceptual framework. We demonstrate that during the early stage of MCI, intestinal ammonia levels are already significantly elevated, whereas blood ammonia remains within the physiological range. More importantly, in the

absence of systemic hyperammonemia, selective elevation of intestinal ammonia can induce MCI-like cognitive deficits in mice. These findings indicate that, at early stages of cognitive impairment, ammonia does not primarily act as a classical toxic metabolite, but rather functions as a gut-derived signaling molecule involved in the regulation of the gut-brain axis. Consistent with this notion, metagenomic and clinical analyses revealed significant enrichment of key urease genes (*ureA*, *ureB*, and *ureC*) in patients with MCI, accompanied by a marked increase in predicted overall urease abundance. Moreover, fecal urease activity and local intestinal ammonia levels were significantly and negatively correlated with MMSE scores. Together, these results indicate that urease-driven ammonia metabolic dysregulation originating from the gut microbiota is activated at an early stage of MCI and influences cognitive function independently of blood ammonia fluctuations. Accordingly, local intestinal metabolic status may reflect cognitive impairment risk earlier and more sensitively than systemic metabolic indicators.

Accumulating evidence has repeatedly highlighted a close association between gut microbiota dysbiosis and cognitive dysfunction [13, 14]. Multiple clinical and animal studies have reported that patients with AD and MCI frequently exhibit elevated blood ammonia levels or abnormalities along the liver-brain axis, leading ammonia to be traditionally viewed as a metabolic by-product that affects the central nervous system via systemic toxicity [15, 16]. However, most of these studies have focused on changes in circulating ammonia and their neurotoxic consequences, leaving unresolved whether ammonia participates in disease initiation as an early local intestinal event. In the present study, we observed that intestinal ammonia levels rise rapidly as early as day 2 after MCI onset, while blood ammonia remains stable throughout. Importantly, because the public metagenomic dataset was derived from an AD cohort, we further validated this intestinal ammonia phenotype in 5xFAD mice. At an early disease stage, 5xFAD mice also showed increased intestinal ammonia levels, supporting the relevance of this local ammonia dysregulation in an AD-related genetic model. These findings help bridge the public AD-associated metagenomic observations and the 5-FU-induced chemotherapy-associated MCI-like model, while indicating that these models should not be considered mechanistically identical. This clear temporal dissociation demonstrates that intestinal ammonia accumulation is not a passive reflection of elevated blood ammonia, but rather a preceding local pathological event. From a temporal and causal perspective, this finding complements and revises the conventional “hyperammonemia-brain injury” paradigm by shifting the primary site of ammonia action forward to the intestinal microenvironment itself [7]. In line with the emerging “microbiota-metabolite-brain” axis framework, cohousing experiments showed that MCI-associated microbiota can transmit an ammonia-related cognitive phenotype to wild-type mice, and FFA rescue further supported the contribution of urease-dependent intestinal ammonia to this effect. Whereas previous studies have predominantly emphasized the roles of inflammatory cytokines, immune signaling, or microbe-derived endotoxins within this axis, our findings directly demonstrate that local gut-derived metabolites themselves can causally drive cognitive dysfunction, thereby providing a more direct and experimentally tractable metabolic signaling model for gut-brain communication [14]. At the microbial level, we found that early MCI is characterized not by nonspecific dysbiosis, but by a directional remodeling toward a high-urease, high-ammonia-producing functional microbial configuration. Notably, gavage experiments revealed that *P. fortuita* markedly elevates intestinal ammonia levels and induces MCI-like cognitive impairment without triggering systemic inflammation. Whereas *Pseudomonas* species have previously been regarded primarily as opportunistic pathogens or inflammation-associated bacteria [17], our findings suggest

that urease-associated ammonia production may contribute to the cognitive effects of *P. fortuita*. FFA treatment reduced intestinal ammonia and improved cognitive performance, although its inhibitory effect on bacterial growth prevents attribution of these benefits specifically to urease inhibition. The urease-expressing recombinant strain provides additional evidence that increased bacterial urease activity can contribute to intestinal ammonia accumulation and cognitive impairment-like phenotypes in mice. These findings indicate that microbial metabolites can influence brain function not only via inflammatory or immune pathways, but also through direct local signaling, thereby identifying mechanistically actionable targets for microbiota-based intervention and highlighting ammonia metabolic modulation as a promising early therapeutic strategy for cognitive disorders.

Previous studies have shown that the TGF-β/SMAD and JAK-STAT signaling pathways play essential roles in neuroinflammation, immune cell differentiation, and cognitive regulation, with Th17-associated pathways in particular recognized as key inflammatory drivers in multiple cognitive and neurodegenerative disorders [18-20]. However, these signaling abnormalities have generally been interpreted as downstream consequences of central or peripheral immune dysregulation, and whether they can be directly triggered by specific gut-derived metabolites during early disease stages has remained unclear. Here, we identify a previously unrecognized pattern of colonic SMAD7 downregulation and brain JAK2 upregulation associated with ammonia-induced cognitive impairment. Distinct from prior studies that rely on systemic hyperammonemia or inflammatory stimuli [12], exogenous ammonium chloride administration significantly elevated intestinal ammonia levels without altering blood ammonia, yet was sufficient to induce stable MCI-like cognitive deficits, consistent with a contribution of local intestinal ammonia to gut-brain interactions. Transcriptomic analyses revealed that the colonic TGF-β signaling pathway and the brain Th17 differentiation pathway are the most ammonia-responsive pathways, characterized by downregulation of SMAD7 and upregulation of JAK2. In vitro experiments further showed that SMAD7 negatively regulates JAK2 protein levels, consistent with the classical understanding of SMAD7 as a negative regulator of TGF-β signaling [21]. Together, these results are consistent with a model in which elevated intestinal ammonia is accompanied by colonic SMAD7 suppression and brain JAK2 upregulation during cognitive impairment. The intermediary signals linking these tissues and the causal contribution of brain JAK2 remain to be determined. At the intervention level, previous studies have reported that probiotics or ammonia-lowering therapies improve neurological function in conditions such as hepatic encephalopathy, with therapeutic efficacy generally attributed to reductions in blood ammonia or suppression of systemic inflammation [22]. Our study further demonstrates that both Limosilactobacillus mucosae supplementation and the clinically used ammonia-lowering agent LOLA significantly restore cognitive function during the early stage of MCI by lowering intestinal ammonia levels, even before blood ammonia becomes elevated. Consistently, 5xFAD mice displayed the same direction of SMAD7-JAK2 alteration, with reduced colonic SMAD7 and increased brain JAK2 expression. Moreover, *L. mucosae* intervention reduced intestinal ammonia, improved behavioral deficits, and restored SMAD7-JAK2 signaling in 5xFAD mice. These results suggest that the intestinal ammonia-SMAD7-JAK2 axis is not restricted to the 5-FU model, but is also modifiable in an AD-related genetic model. These findings underscore that local intestinal metabolic modulation alone is sufficient to confer neurofunctional benefit.

Although our data support a colon SMAD7-brain JAK2 signaling axis, the anatomical route linking

colonic ammonia-responsive signaling to brain JAK2 activation remains unresolved. The vagus nerve represents a plausible candidate pathway because it regulates intestinal immune homeostasis and cholinergic anti-inflammatory signaling [23], and vagotomy has been shown to abolish certain microbiota-dependent effects on brain neurotransmitter receptor expression and behavior [24]. Thus, ammonia-induced suppression of colonic SMAD7 may potentially engage vagus-dependent neuroimmune signaling to promote brain JAK2 activation. However, because vagotomy experiments were not performed in this study, we cannot determine whether this pathway is vagus-dependent. Moreover, vagotomy does not eliminate all immunological components of the gut-brain axis, as circulating cytokines, peripheral immune activation, intestinal barrier dysfunction, and humoral/metabolic signals may also mediate gut-to-brain communication. This issue warrants further investigation using subdiaphragmatic vagotomy and immune profiling.

Several limitations should be acknowledged. First, the clinical cohort size is relatively limited, and future validation in large, multicenter cohorts will be required to confirm the association between intestinal ammonia and cognitive function. In addition, all participants were recruited from the same elderly care facility and received broadly standardized meals; however, individual-level quantitative dietary intake was not available, and diet, particularly animal-protein intake, could not be formally included as a covariate in the analysis. Second, although MCI-like cognitive phenotypes were robustly reproduced in mice, species differences between animal models and human cognitive disorders necessitate further translational validation. The 5-FU-induced model should be interpreted as a chemotherapy-associated MCI-like model and may not fully represent age-related neurodegenerative cognitive impairment. Although our low-dose, low-frequency 5-FU regimen did not cause overt mucosal damage by H&E staining and FFA rescue supported a contribution of urease-dependent intestinal ammonia, ammonia-independent effects of 5-FU cannot be fully excluded. Third, although colonic SMAD7 restoration improved behavior and was accompanied by lower brain JAK2, these experiments do not establish a direct SMAD7-to-JAK2 signaling pathway across organs or demonstrate that brain JAK2 is required for the behavioral effects. The intervening neural, immune, or humoral signals, as well as other pathways that may contribute to cognitive impairment, require further investigation. In addition, inter-individual variability in the gut microbiota may influence intervention efficacy, warranting more refined multi-omics-based analyses in future studies.

In summary, our study systematically reveals a critical role for gut microbiota-derived urease-driven ammonia metabolic dysregulation in the early stage of MCI, identifies intestinal ammonia as an early functional contributor to cognitive impairment, and identifies colonic SMAD7 and brain JAK2 as associated molecular changes that may participate in the response to intestinal ammonia. Targeting intestinal ammonia, either through probiotic intervention or pharmacological modulation, effectively improves cognitive function and supports a proof-of-concept ammonia-targeting intervention strategy. These findings not only expand the theoretical framework of the gut-brain axis in neurodegenerative disease research, but also provide new avenues for early diagnosis, microbiota-based intervention, and pathway-targeted therapy in MCI. Future studies should explore personalized microbiome-based interventions, long-term efficacy, and combination therapeutic strategies to enable more precise and effective prevention and treatment of MCI.

Methods

Collection and analysis of fecal metagenomic data from public cognitive impairment-related cohorts and 5-FU-treated cohorts

Publicly available fecal metagenomic datasets from an AD-associated cohort were analyzed to assess gut microbial urease genes and ammonia-producing potential [25]. A paired dataset comprising fecal samples collected before and after 5-FU treatment was additionally analyzed to determine whether 5-FU exposure alone altered these microbial functions [26]. Dataset characteristics and detailed bioinformatic procedures are provided in **SI Appendix, Materials and Methods**.

Recruitment, biospecimen collection, and clinical analyses

An independent cohort of 20 healthy controls and 28 participants with MCI was recruited. Cognitive performance was assessed using the MMSE and MoCA, and demographic and clinical characteristics were recorded. Participants receiving medications or treatments likely to affect the gut microbiota were excluded. All participants lived in the same elderly care facility and received broadly standardized meals. Written informed consent was obtained from all participants, and the study was approved by the Institutional Review Board of the School of Basic Medical Science, Central South University (No. 2021-KT75). Peripheral blood was collected for plasma Aβ42 measurement and APOE genotyping based on rs429358 and rs7412. Detailed recruitment criteria, sample-processing procedures, and analytical methods are provided in **SI Appendix, Materials and Methods.**

Fecal sample collection and measurement of fecal ammonia and urease activity

Fresh fecal samples were collected in sterile airtight tubes, transported on ice, and stored at -80 °C. Samples were thawed once, weighed, homogenized in prechilled extraction buffer, and centrifuged at 4 °C. Fecal ammonia concentrations and urease activity were measured using commercial assay kits. Detailed procedures are provided in **SI Appendix, Materials and Methods.**

Animals and housing conditions

Ten-week-old male SPF Kunming mice were used for the 5-FU-induced MCI-like model, NH_4Cl treatment, and bacterial intervention experiments, whereas 8-week-old male 5xFAD mice and age-matched controls were used for AD-related validation. Mice were housed under controlled conditions with free access to standard chow and water. All animal procedures were approved by the Institutional Ethics Committee for Animal Procedures of Central South University (CSU-2024-0315). Detailed animal sources, housing conditions, and diet composition are provided in **SI Appendix, Materials and Methods**.

Establishment and assessment of the MCI mouse model

MCI was induced in Kunming mice by intraperitoneal administration of 5-FU (SOUTHWESTPHARMACEUTICAL, CO,.LTD.) at 25 mg/kg body weight in 0.2 mL PBS , twice weekly for two consecutive weeks [27]. Cognitive deficits were evaluated using a battery of behavioral tests. Following completion of the experiments, mice were euthanized by cervical dislocation. Colonic contents were harvested and immediately snap-frozen for subsequent determination of ammonia levels and urease activity. Colon and brain tissues were also rapidly frozen in liquid nitrogen and stored for further analyses.

Hematoxylin and eosin staining

To evaluate whether the 5-FU regimen used in this study caused overt intestinal mucosal injury, colon tissues were collected for histopathological analysis. Fresh colon tissues were rinsed gently with PBS, fixed in 4% paraformaldehyde, embedded in paraffin, sectioned, and subjected to H&E staining using standard procedures. Stained sections were scanned using a NanoZoomer S360 digital slide scanner.

Co-housing and urease-inhibition rescue

WT mice were co-housed with MCI-like mice to assess microbiota-mediated transmission of intestinal ammonia accumulation and cognitive impairment. To evaluate the contribution of bacterial urease, cohoused WT mice were treated with FFA (6 mg/kg, intraperitoneally) or vehicle. Fecal ammonia levels and cognitive performance were subsequently assessed. Detailed experimental procedures are provided in **SI Appendix, Materials and Methods.**

Assessment of cognitive function

Cognitive performance was evaluated using the Y-maze, novel object recognition, and Morris water maze tests to assess spatial working memory, recognition memory, and spatial learning and memory, respectively. Behavioral testing was conducted under standardized conditions, and the relevant exploration indices, escape latencies, and platform-crossing frequencies were recorded. Detailed procedures and calculation methods are provided in **SI Appendix, Materials and Methods.**

Sample collection

Fecal samples were obtained one day prior to euthanasia by gentle anal stimulation using sterile cotton swabs. Samples were immediately snap-frozen in liquid nitrogen and stored at -80 ℃ until further analysis. Blood samples were collected from the orbital venous plexus under isoflurane anesthesia before euthanasia by cervical dislocation and stored at -80 ℃. Colon and brain tissues were rinsed with PBS and processed according to the requirements of subsequent biochemical assays.

Metagenomic and transcriptomic analyses

Fecal microbial DNA and total RNA from colon and brain tissues were extracted and subjected to paired-end sequencing. Metagenomic reads were quality-filtered, assembled, and analyzed for taxonomic composition, functional genes, KEGG pathways, and bacterial contributors to urease genes. RNA-seq reads were aligned to the mouse reference genome, followed by differential expression and gene set enrichment analyses. Statistical testing of metagenomic features included false-discovery rate correction. Detailed sequencing and bioinformatic procedures are provided in **SI Appendix, Materials and Methods**.

Drug preparation and animal treatments

The drugs used in this study and their administration regimens are summarized as follows. Specifically, FFA (Ambeed) was dissolved in 0.1% DMSO in PBS and administered intraperitoneally at 6 mg/kg. NH_4Cl (Sinopharm) was dissolved in PBS and gavaged at 180 mg/kg body weight. LOLA (Macklin) was dissolved in PBS and fed at 100 mg/kg body weight. Unless otherwise indicated, PBS served as the vehicle control. All drug dosages were normalized to body

weight, and treatments were administered at a fixed volume of 0.2 mL per dose.

Quantification of biochemical parameters

Fecal ammonia was quantified using the Ammonia Content Assay Kit (G0436W, Grace Biotechnology). Blood ammonia levels was quantified using the Blood Ammonia Content Assay Kit (BC4385, Solarbio, Beijing, China). Fecal urease activity was determined with the Urease (UE)Activity Assay Kit (BC4115, Solarbio, Beijing, China). All assays were performed according to the manufacturer's protocols.

Isolation of urease-positive bacteria

Urease-positive bacteria were isolated from fecal samples of participants with MCI using urea phenol red agar. Colonies showing urease-associated color changes were purified, identified by full-length 16S rRNA gene sequencing, and stored at -80 °C for subsequent experiments. Detailed isolation and identification procedures are provided in **SI Appendix, Materials and Methods.**

Construction of urease-expressing recombinant *E. coli*

Recombinant Escherichia coli BL21(DE3) expressing the *Lysinibacillus fusiformis* ureABC genes was constructed and validated by protein electrophoresis and mass spectrometry [28]. Following antibiotic pretreatment, mice were orally administered the recombinant strain or the corresponding empty-vector control. Detailed construction, validation, culture, and administration procedures are provided in **SI Appendix, Materials and Methods.**

***P. fortuita* intervention and urease-inhibition assays**

Following antibiotic pretreatment, mice were orally administered urease-positive bacterial strains, including *E. faecium*, *K. oxytoca*, and *P. fortuita*. To assess the contribution of urease activity, *P. fortuita*-treated mice received FFA (6 mg/kg, intraperitoneally) or vehicle, followed by measurement of fecal ammonia and cognitive performance. The effects of FFA on *P. fortuita* growth, urease activity, and ammonia production were additionally evaluated in vitro. Fecal *P. fortuita* and *P. fortuita*-derived urease gene abundance were quantified by qPCR using bacterial 16S rRNA as the reference. Detailed bacterial culture, intervention, biochemical assay, primer, and qPCR procedures are provided in **SI Appendix, Materials and Methods**.

Cell culture

HEK293FT, NIH3T3, Caco-2, C8-D1A, and IMCCs were maintained under standard culture conditions at 37 °C with 5% CO_2. Cells were cultured in the appropriate serum-supplemented DMEM or supplier-recommended complete medium. Detailed cell sources and culture conditions are provided in **SI Appendix, Materials and Methods**.

Transwell epithelial cell-astrocyte co-culture assay

IMCCs transfected with a SMAD7 overexpression plasmid or empty vector were cultured in the upper chamber of Transwell inserts, with C8-D1A astrocytes in the lower chamber. After 48 h of indirect co-culture, C8-D1A cells were collected, and JAK2 protein expression was assessed by western blotting. Detailed procedures are provided in **SI Appendix, Materials and Methods.**

Western blot analysis

Cell lysates were separated by SDS-PAGE and transferred to PVDF membranes. Proteins were detected using antibodies against SMAD7, JAK2, Flag, and GAPDH, followed by chemiluminescence imaging and densitometric analysis with ImageJ. GAPDH was used as the loading control. Detailed antibody information and experimental procedures are provided **in SI Appendix, Materials and Methods.**

Cellular immunofluorescence staining

Cells were fixed, permeabilized, and stained with antibodies against SMAD7, JAK2, Flag, or HA, followed by fluorescent secondary antibodies and DAPI counterstaining. Images were acquired using an inverted fluorescence microscope, and fluorescence intensity was quantified with ImageJ. Detailed antibody information and staining procedures are provided in **SI Appendix, Materials and Methods.**

Plasmid transfection

Cells at 70-80% confluence were transfected with SMAD7 and/or JAK2 expression plasmids using Vigofect reagent. Cells were collected 24 h after transfection for subsequent analyses. Detailed transfection conditions are provided in **SI Appendix, Materials and Methods.**

AAV-mediated colonic SMAD7 overexpression

An AAV9 vector expressing 3×Flag-tagged mouse Smad7 under the Villin promoter was used to restore intestinal epithelial SMAD7 expression. Following establishment of the 5-FU-induced MCI-like model, mice received AAV-SMAD7 or control AAV by rectal administration. Cognitive performance was subsequently assessed, and colonic SMAD7 and brain JAK2 protein levels were evaluated by western blotting. Detailed vector construction, viral dosage, administration, and validation procedures are provided in **SI Appendix, Materials and Methods.**

***L. mucosae* intervention and ammonia-lowering validation**

Live *L. mucosae*, heat-killed *L. mucosae*, and live *L. fermentum* were compared to assess the dependence and strain specificity of ammonia lowering. Their ammonia-assimilating capacities were evaluated in vitro in medium containing NH_4Cl and glucose. Following antibiotic pretreatment, mice received the corresponding bacterial preparations by oral gavage, after which fecal ammonia levels and cognitive performance were assessed. Detailed bacterial preparation, culture, intervention, and assay procedures are provided in **SI Appendix, Materials and Methods.**

Statistical analysis

Animals were randomly assigned to experimental groups, and data collection was performed in a randomized manner. Investigators were blinded to group allocation during both the collection and analysis of data. Sample sizes were chosen based on prior experience and previous studies conducted in our laboratory. Statistical analyses were conducted using R software, with specific packages indicated in the corresponding Methods sections. Statistical significance was assessed using a two-tailed Student's t-test for comparisons between two groups or one-way ANOVA followed by Fisher's LSD post hoc test for comparisons involving three or more groups. Each data point corresponds to an independent biological replicate, and all experiments were performed with a minimum of three independent biological replicates.

Data Availability

Metagenomic sequencing data and RNA-seq data are available in the Genome Sequence Archive (https://ngdc.cncb.ac.cn/gsa/), under accession number CRA062809 and CRA062810.

Acknowledgements

We thank the Top-Notch Innovation Base of Basic Medicine, Central South University, for providing access to the upright fluorescence microscope (Leica DM3000 LED) used in this study. We thank Shuishi Li and Yin Shi (Xiangya Hospital Central South University) for their dedicated assistance and support with sample sequencing, clinical follow-up, and expert consultation throughout the conduct of this study.

Fundings

This work was funded by the National Natural Science Foundation of China (32300051 to J.H., 32170071 to Z.Y.) and Natural Science Foundation of Hunan Province (2025JJ50101 to Z.Y.).

Author Contributions Statement

Z.Y., K.G. and J.H. designed the research. H.C., Z.W., and J.T. performed experiments. H.C., Z.W., Y.L. and L.K. completed sample and data collection. H.C., Z.W., and J.H. analyzed and visualized the data. H.C. and Z.W. wrote the draft. H.C., J.H., and Z.Y. wrote and edited the final manuscript. All authors contributed to the article and approved the submitted version.

Competing Interests Statement

The authors declare that they have no competing interests.

Figure legend

Figure 1 Gut microbial urease activity is associated with early intestinal ammonia accumulation during cognitive impairment. (**A**) Workflow for fecal metagenomic collection and analysis in the public population-based cohort and the independent clinical cohort. (**B**) Changes in the abundance of urease genes in the public population-based cohort. (**C**) Changes in the abundance of urease genes in the clinical cohort. (**D**) Comparative analysis of urease gene abundance between the public population-based cohort and the clinical cohort. (**E**) Alterations in fecal urease activity in the clinical cohort. (**F**) Correlation analysis between fecal urease activity and MMSE scores. (**G**) Changes in fecal ammonia levels in the clinical cohort. (**H**) Correlation analysis between fecal ammonia levels and MMSE scores. **(I)** Experimental timeline for establishment and behavioral evaluation of the 5-FU-induced chemotherapy-associated MCI-like mouse model. (**J**) Changes in urease gene abundance in fecal metagenomes from WT and 5-FU-induced MCI-like mice. (**K**) Relative abundance of urease genes in mouse fecal metagenomes across experimental groups. (**L**) Temporal dynamics of fecal ammonia levels during MCI-like model establishment. (**M**) Changes in blood ammonia levels during MCI-like model establishment. (**N**) Experimental strategy of the cohousing assay between WT and MCI-like mice. (**O**) Dynamic changes in intestinal ammonia levels following cohousing. (**P**) Changes in cognitive performance assessed by the novel object recognition test. (**Q**) Heatmap depicting the spatial distribution of residence time in the test arena. (**R**) Residence time in the target area during testing and changes in spontaneous alternation ratio in the Y-maze test. (**S**) Latency to locate the hidden platform during acquisition training in the Morris water maze test. (**T**) Representative swim paths during the probe trial (60 s) following platform removal. (**U**) Number of platform location crossings during the probe trial. All data are presented as mean ± s.d. from at least three biologically independent experiments. Statistical significance was assessed using two-tailed Student's t-test.

Figure 2 Urease-positive bacterial isolates drive MCI-like cognitive phenotypes via urease-dependent ammonia production. (**A**) Source tracking analysis of bacterial hosts contributing urease genes. (**B**) Strategy for the isolation of urease-positive bacterial strains. (**C**) Taxonomic summary of urease-positive isolates. (**D**) Changes in the abundance of urease-positive isolates in mouse fecal metagenomes. (**E**) Changes in intestinal ammonia levels in WT mice following bacterial strain administration. (**F**) Changes in blood ammonia levels in WT mice following bacterial strain administration. (**G**) Behavioral performance normalized by Z-score and cumulative cognitive scores after bacterial strain intervention. (**H**) Schematic illustration of the experimental design for Pf combined with FFA treatment. (**I**) Changes in intestinal ammonia levels after Pf plus FFA intervention. (**J**) Changes in spontaneous alternation ratio in the Y-maze test following Pf plus FFA intervention. (**K**) Changes in cognitive index derived from the novel object recognition test following Pf plus FFA intervention. (**L**) Latency to locate the hidden platform during acquisition training in the Morris water maze test following Pf plus FFA intervention. (**M**) Number of platform location crossings during the probe trial after platform removal following Pf plus FFA intervention. (**N**) Experimental design for mouse intervention with heterologous urease-expressing *E. coli* (urease_BL21). (**O**) Changes in intestinal ammonia levels following urease_BL21 intervention. (**P**) Changes in spontaneous alternation ratio in the Y-maze test following urease_BL21 intervention. (**Q**) Changes in cognitive index derived from the novel object recognition test following

urease_BL21 intervention. (**R**) Latency to locate the hidden platform during acquisition training in the Morris water maze test following urease_BL21 intervention. (**S**) Number of platform location crossings during the probe trial after platform removal following urease_BL21 intervention. All data are presented as mean ± s.d. from at least three biologically independent experiments. Statistical significance was assessed using two-tailed Student's t-test.

Figure 3 Intestinal ammonia contributes to MCI-like cognitive impairment through colonic SMAD7 suppression and brain JAK2 activation. (**A**) Schematic illustration of the experimental design for NH_4Cl administration in mice. (**B**) Changes in intestinal ammonia levels following NH_4Cl treatment. (**C**) Changes in blood ammonia levels following NH_4Cltreatment. (**D**) Changes in spontaneous alternation ratio in the Y-maze test following NH_4Cltreatment. (**E**) Changes in cognitive index derived from the novel object recognition test following NH_4Cl treatment. (**F**) Latency to locate the hidden platform during acquisition training in the Morris water maze test following NH_4Cltreatment. (**G**) Number of platform location crossings during the probe trial after platform removal following NH_4Cltreatment. (**H**) GSEA of the Th17 cell differentiation pathway in brain transcriptomes from WT and NH_4Cl-treated mice. (**I**) GSEA of the TGF-β signaling pathway in colonic transcriptomes from WT and NH_4Cl-treated mice. (**J**) Heatmap showing Z-score-normalized expression patterns of colonic *Smad7* and brain *Jak2* in WT, NH_4Cl-treated, and 5-FU-induced MCI-like mice. (**K**) Immunoblot analysis of SMAD7 expression in Caco-2 intestinal epithelial cells exposed to the indicated concentrations of NH_4Cl. (**L**) Schematic representation of the Transwell co-culture system. IMCCs overexpressing SMAD7 were placed in the upper chamber, and C8-D1A astrocytes were cultured in the lower chamber. (**M**) Immunoblot analysis of JAK2 expression in C8-D1A astrocytes after co-culture with IMCCs transfected with Flag-SMAD7 or the corresponding empty vector. (**N**) Immunoblot analysis of brain JAK2 expression in NH_4Cl-treated mice and 5-FU-induced MCI-like mice, with the corresponding WT controls. (**O**) Experimental timeline and group allocation for AAV-mediated restoration of colonic SMAD7 expression. After establishment of the 5-FU-induced MCI-like model, mice received AAV-Flag-SMAD7 or the corresponding AAV-Flag-vector by rectal administration, followed by an expression period and behavioral testing. (**P)** Immunoblot analysis of colonic SMAD7 and brain JAK2 protein levels in MCI-like mice treated with AAV-Flag-SMAD7 or the corresponding vector control. (**Q**) Spontaneous alternation percentages in the Y-maze test following AAV-mediated SMAD7 restoration. (**R**) Recognition index in the novel object recognition test. (**S**) Escape latency during the acquisition phase of the Morris water maze test. (**T**) Number of crossings over the previous platform location during the probe trial. All data are presented as mean ± s.d. from at least three biologically independent experiments. Statistical significance was assessed using a two-tailed Student's t-test for comparisons between two groups, or one-way ANOVA followed by Fisher's LSD post hoc test for comparisons involving three or more groups.

Figure 4 ***Limosilactobacillus mucosae attenuates intestinal ammonia accumulation and cognitive impairment-like phenotypes across experimental models.*** (**A**) Source tracking analysis of bacterial hosts contributing urease. (**B**) Workflow for the identification of ammonia assimilation genes and heatmap showing the relative abundance of ammonia assimilation genes within the order Lactobacillales. (**C**) Changes in the relative abundance of Lactobacillales in MCI mice. (**D**) Schematic illustration of the experimental design for *L. mucosae* administration in MCI mice. (**E**) Changes in fecal ammonia levels following *L. mucosae* intervention in MCI mice. (**F**) Changes in

spontaneous alternation ratio in the Y-maze test following *L. mucosae* intervention. (**G**) Changes in cognitive index derived from the novel object recognition test following *L. mucosae* intervention. (**H**) Latency to locate the hidden platform during acquisition training in the Morris water maze test following *L. mucosae* intervention. (**I**) Number of platform location crossings during the probe trial after platform removal following Limosilactobacillus mucosae intervention. (**J**) Immunoblot analysis of SMAD7 expression from colon and JAK2 expression from brain in *L. mucosae*-treated MCI mice. (**K**) Experimental timeline for comparing live *L. mucosae* (Lm), heat-killed *L. mucosae* (HK-Lm), and live *L. fermentum* (Lf) in 5-FU-induced MCI-like mice. (**L**) Fecal ammonia concentrations in untreated MCI-like mice and MCI-like mice treated with live Lm, HK-Lm, or live Lf. (**M**) Spontaneous alternation percentages in the Y-maze test. (**N**) Recognition index in the novel object recognition test. (**O**) Escape latency during the acquisition phase of the Morris water maze test. (**P**) Number of crossings over the previous platform location during the probe trial. (**Q**) Experimental timeline for live *L. mucosae* intervention in 5xFAD mice. (**R**) Fecal ammonia concentrations in WT, untreated 5xFAD, and *L. mucosae*-treated 5xFAD mice. (**S**) Spontaneous alternation percentages in the Y-maze test. (**T**) Recognition index in the novel object recognition test. (**U**) Escape latency during the acquisition phase of the Morris water maze test. (**V**) Number of crossings over the previous platform location during the probe trial. (**W**) Representative immunoblot analysis of colonic SMAD7 and brain JAK2 protein levels in WT, untreated 5xFAD, and *L. mucosae*-treated 5xFAD mice. All data are presented as mean ± s.d. from at least three biologically independent experiments. Statistical significance was assessed using a two-tailed Student's t-test for comparisons between two groups, or one-way ANOVA followed by Fisher's LSD post hoc test for comparisons involving three or more groups.

References list

1. Aarsland, D., et al., Parkinson disease-associated cognitive impairment. *Nat Rev Dis Primers*, 2021. **7**(1): 47.

2. Wilson, D.M., 3rd, et al., Hallmarks of neurodegenerative diseases. *Cell*, 2023. **186**(4): 693-714.

3. Huszar, Z., et al., Risk of conversion to mild cognitive impairment or dementia among subjects with amyloid and tau pathology: a systematic review and meta-analysis. *Alzheimers Res Ther*, 2024. **16**(1): 81.

4. Selkoe, D.J. and J. Hardy, The amyloid hypothesis of Alzheimer's disease at 25 years. *EMBO Mol Med*, 2016. **8**(6): 595-608.

5. Mayer, E.A., K. Nance, and S. Chen, The Gut-Brain Axis. *Annu Rev Med*, 2022. **73**: 439-453.

6. Chen, G., et al., Novel roles of ammonia in physiology and cancer. *J Mol Cell Biol*, 2025. **17**(1).

7. Jakhar, D., Sarin, S.K., Kaur, S., Gut microbiota and dynamics of ammonia metabolism in liver disease. *npj Gut Liver*, 2024. **1**(11).

8. Shen, T.C., et al., Engineering the gut microbiota to treat hyperammonemia. *J Clin Invest*, 2015. **125**(7): 2841-50.

9. Wang, P., et al., Gut microbiome-derived ammonia modulates stress vulnerability in the host. *Nat Metab*, 2023. **5**(11): 1986-2001.

10. Dasarathy, S., et al., Ammonia toxicity: from head to toe? *Metab Brain Dis*, 2017. **32**(2): 529-538.

11. Rose, C.F., et al., Hepatic encephalopathy: Novel insights into classification, pathophysiology and therapy. *J Hepatol*, 2020. **73**(6): 1526-1547.

12. Jayakumar, A.R. and M.D. Norenberg, Hyperammonemia in Hepatic Encephalopathy. *J Clin Exp Hepatol*, 2018. **8**(3): 272-280.

13. Kolobaric, A., et al., Gut microbiome predicts cognitive function and depressive symptoms in late life. *Mol Psychiatry*, 2024. **29**(10): 3064-3075.

14. Loh, J.S., et al., Microbiota-gut-brain axis and its therapeutic applications in neurodegenerative diseases. *Signal Transduct Target Ther*, 2024. **9**(1): 37.

15. Adlimoghaddam, A., M.G. Sabbir, and B.C. Albensi, Ammonia as a Potential Neurotoxic Factor in Alzheimer's Disease. *Front Mol Neurosci*, 2016. **9**: 57.

16. Chen, T., et al., Metabolic phenotyping reveals an emerging role of ammonia abnormality in Alzheimer's disease. *Nat Commun*, 2024. **15**(1): 3796.

17. Qin, S., et al., Pseudomonas aeruginosa: pathogenesis, virulence factors, antibiotic resistance, interaction with host, technology advances and emerging therapeutics. *Signal Transduct Target Ther*, 2022. **7**(1): 199.

18. Fu, J., et al., The role of Th17 cells/IL-17A in AD, PD, ALS and the strategic therapy targeting

on IL-17A. *J Neuroinflammation*, 2022. **19**(1): 98.

19. von Bernhardi, R., F. Cornejo, G.E. Parada, and J. Eugenin, Role of TGFbeta signaling in the pathogenesis of Alzheimer's disease. *Front Cell Neurosci*, 2015. **9**: 426.

20. Yan, Z., et al., Role of the JAK/STAT signaling pathway in regulation of innate immunity in neuroinflammatory diseases. *Clin Immunol*, 2018. **189**: 4-13.

21. Yan, X., Z. Liu, and Y. Chen, Regulation of TGF-beta signaling by Smad7. *Acta Biochim Biophys Sin (Shanghai)*, 2009. **41**(4): 263-72.

22. Dalal, R., R.G. McGee, S.M. Riordan, and A.C. Webster, Probiotics for people with hepatic encephalopathy. *Cochrane Database Syst Rev*, 2017. **2**(2): CD008716.

23. Matteoli, G. and G.E. Boeckxstaens, The vagal innervation of the gut and immune homeostasis. *Gut*, 2013. **62**(8): 1214-22.

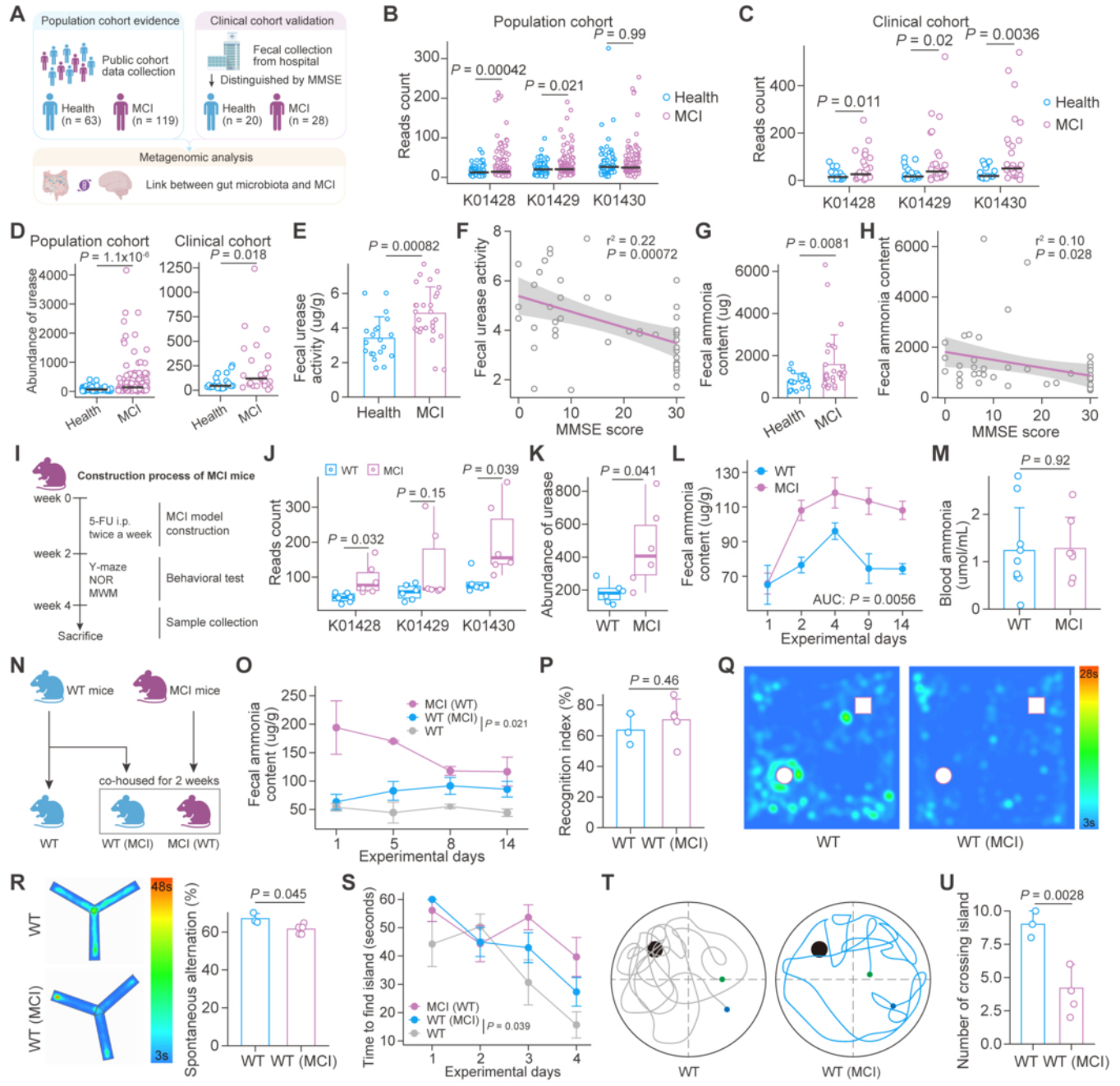
24. Bravo, J.A., et al., Ingestion of Lactobacillus strain regulates emotional behavior and central GABA receptor expression in a mouse via the vagus nerve. *Proc Natl Acad Sci U S A*, 2011. **108**(38): 16050-5.

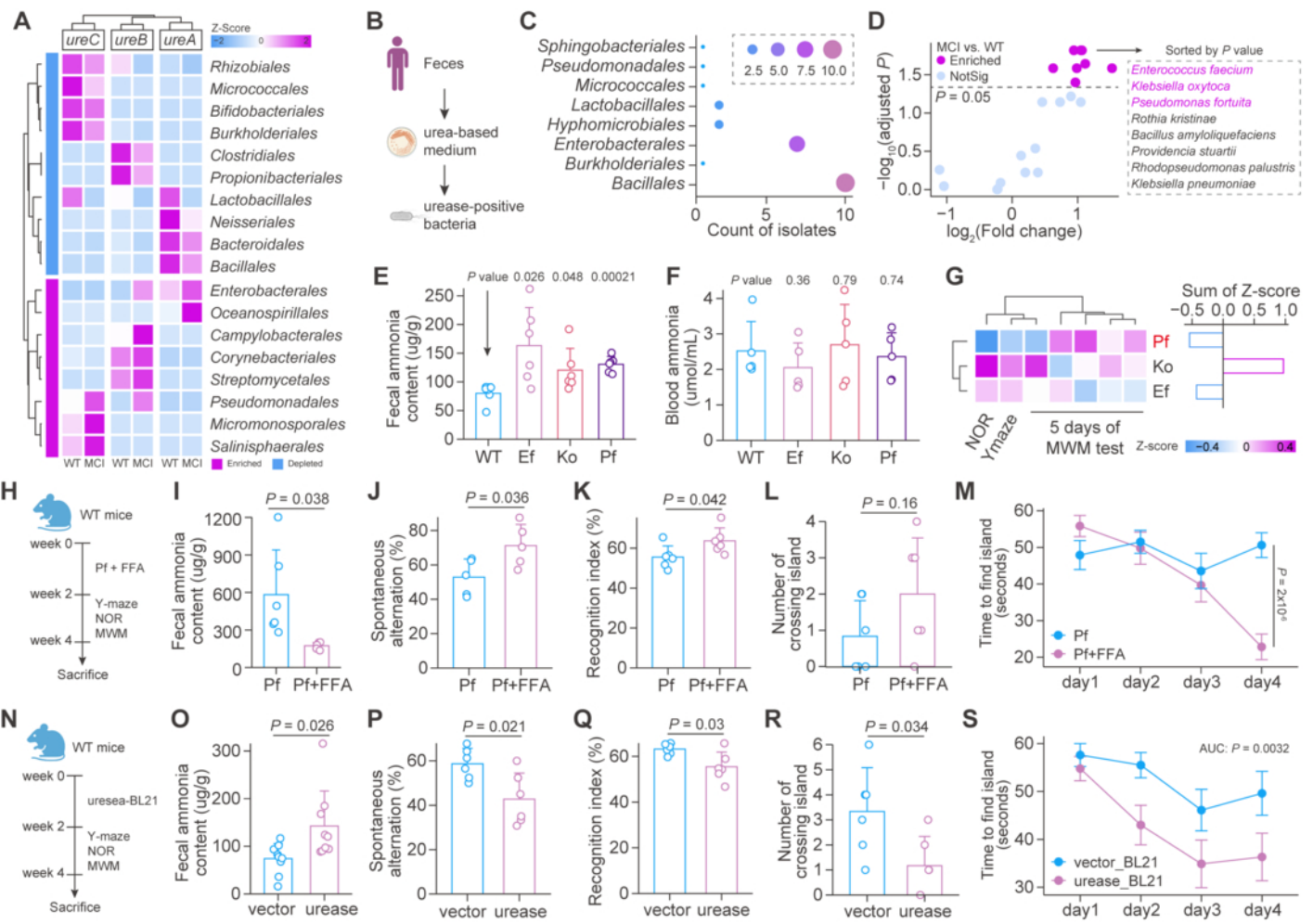
25. Jia, L., et al., Metagenomic analysis characterizes stage-specific gut microbiota in Alzheimer's disease. *Mol Psychiatry*, 2025. **30**(9): 3951-3962.

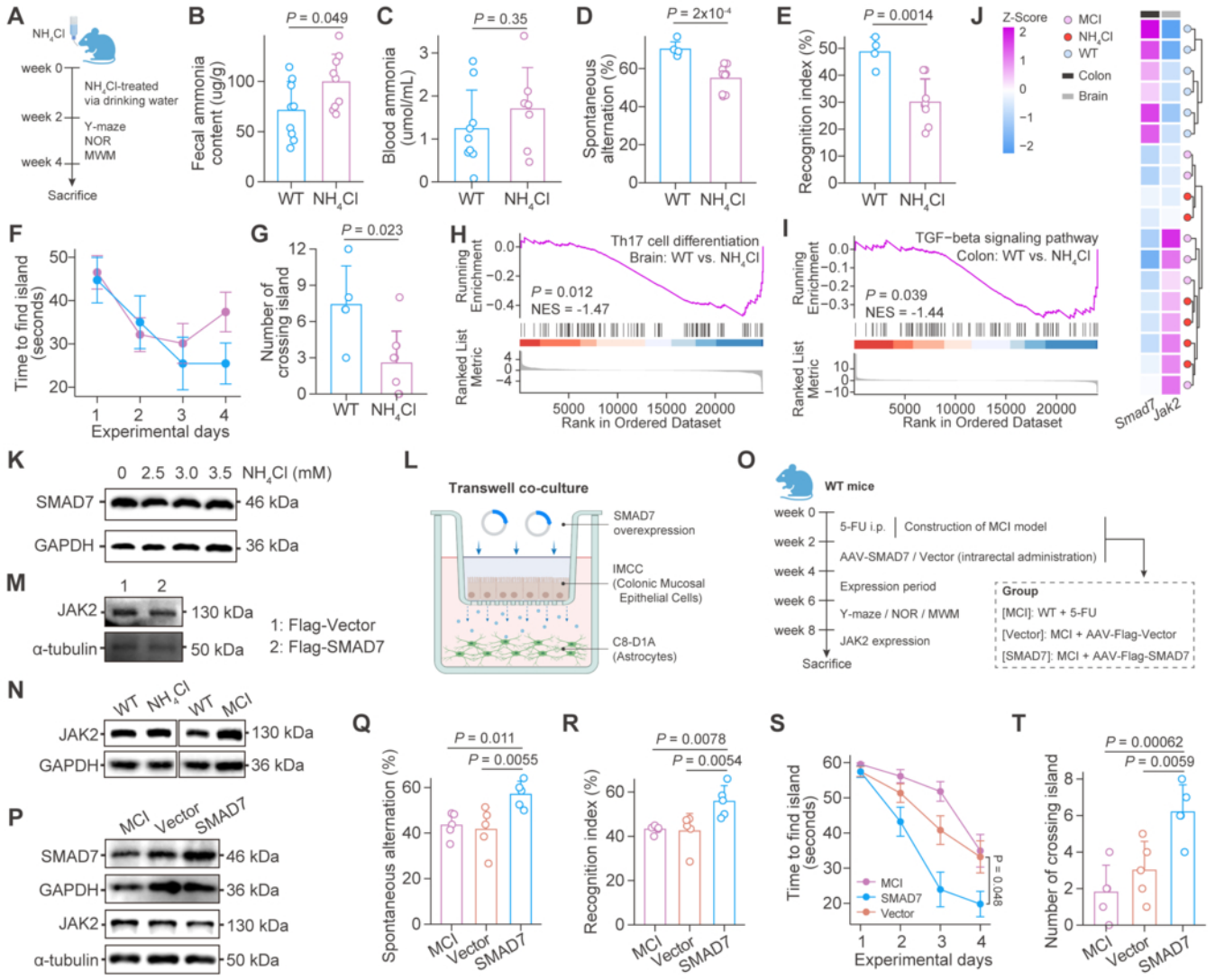
26. Wan, L., et al., Mutational Pattern Induced by 5-Fluorouracil and Oxaliplatin in the Gut Microbiome. *Front Microbiol*, 2022. **13**: 841458.

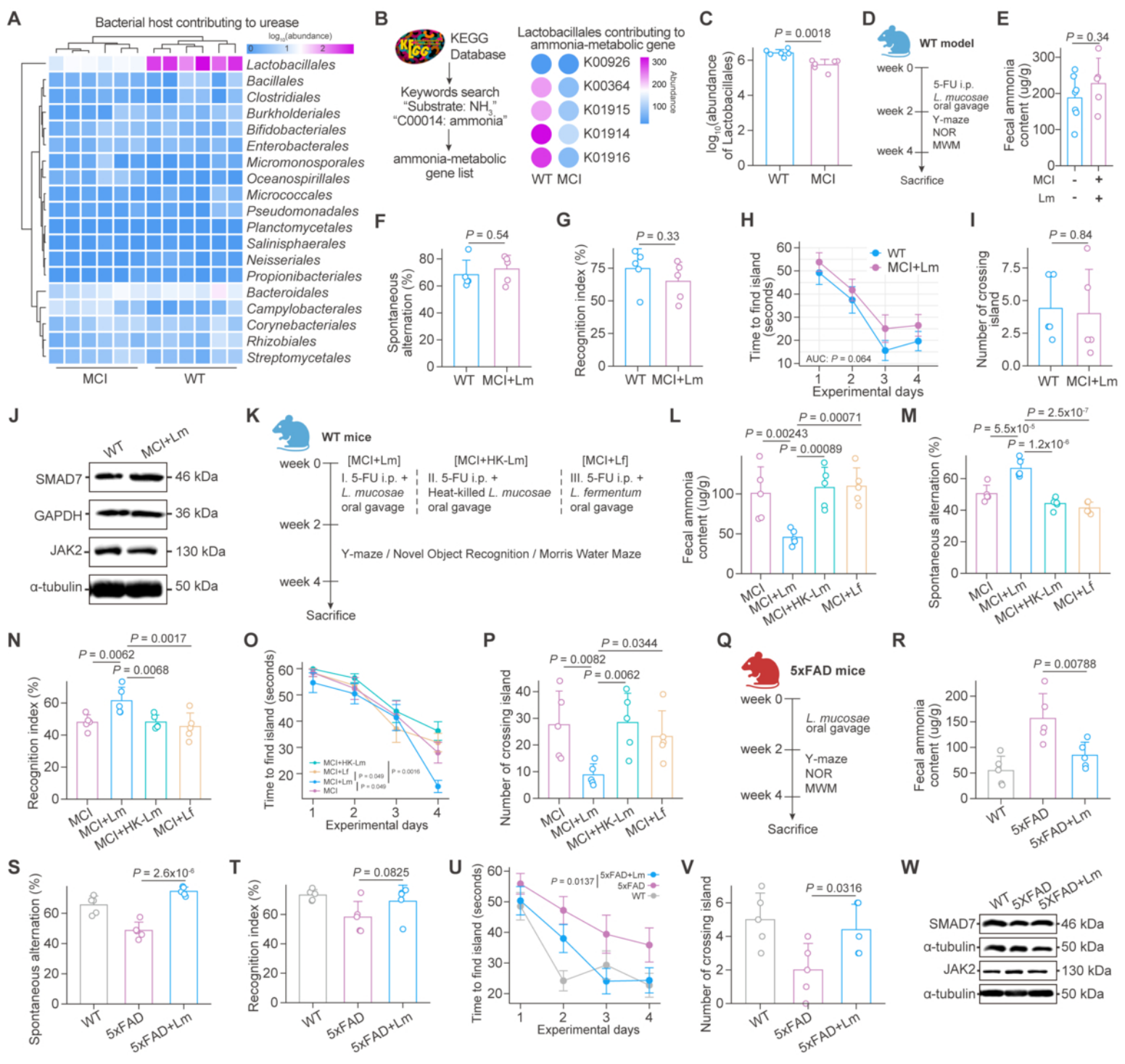
27. Abulizi, A., et al., Ganoderic acid improves 5-fluorouracil-induced cognitive dysfunction in mice. *Food Funct*, 2021. **12**(24): 12325-12337.

28. Chen, H., et al., Gut microbial ammonia enhances colonic acetylcholine levels to regulate intestinal motility. *Nat Microbiol*, 2026. **11**(4): 907-919.


A
Population cohort evidence
Public cohort data collection
Health (n = 63)
MCI (n = 119)
Clinical cohort validation
Fecal collection from hospital
Distinguished by MMSE
Health (n = 20)
MCI (n = 28)
Metagenomic analysis
Link between gut microbiota and MCI
B
Population cohort
Reads count
P = 0.00042
P = 0.021
P = 0.99
Health
MCI
K01428
K01429
K01430
C
Clinical cohort
Reads count
P = 0.011
P = 0.02
P = 0.0036
Health
MCI
K01428
K01429
K01430
D
Population cohort
P = 1.1x10⁻⁶
Clinical cohort
P = 0.018
Abundance of urease
Health
MCI
E
P = 0.00082
Fecal urease activity (ug/g)
Health
MCI
F
r² = 0.22
P = 0.00072
Fecal urease activity
MMSE score
G
P = 0.0081
Fecal ammonia content (ug)
Health
MCI
H
r² = 0.10
P = 0.028
Fecal ammonia content
MMSE score
I
Construction process of MCI mice
week 0
5-FU i.p. twice a week
MCI model construction
week 2
Y-maze NOR MWM
Behavioral test
week 4
Sacrifice
Sample collection
J
WT
MCI
P = 0.032
P = 0.15
P = 0.039
Reads count
K01428
K01429
K01430
K
P = 0.041
Abundance of urease
WT
MCI
L
WT
MCI
Fecal ammonia content (ug/g)
AUC: P = 0.0056
Experimental days
M
P = 0.92
Blood ammonia (umol/mL)
WT
MCI
N
WT mice
MCI mice
co-housed for 2 weeks
WT
WT (MCI)
MCI (WT)
O
MCI (WT)
WT (MCI)
WT
P = 0.021
Fecal ammonia content (ug/g)
Experimental days
P
P = 0.46
Recognition index (%)
WT
WT (MCI)
Q
28s
3s
WT
WT (MCI)
R
WT
WT (MCI)
48s
3s
P = 0.045
Spontaneous alternation (%)
WT
WT (MCI)
S
MCI (WT)
WT (MCI)
WT
P = 0.039
Time to find island (seconds)
Experimental days
T
WT
WT (MCI)
U
P = 0.0028
Number of crossing island
WT
WT (MCI)


A
ureC
ureB
ureA
Z-Score
Rhizobiales
Micrococcales
Bifidobacteriales
Burkholderiales
Clostridiales
Propionibacteriales
Lactobacillales
Neisseriales
Bacteroidales
Bacillales
Enterobacterales
Oceanospirillales
Campylobacterales
Corynebacteriales
Streptomycetales
Pseudomonadales
Micromonosporales
Salinisphaerales
WT MCI WT MCI WT MCI
Enriched
Depleted
B
Feces
urea-based medium
urease-positive bacteria
C
Sphingobacteriales
Pseudomonadales
Micrococcales
Lactobacillales
Hyphomicrobiales
Enterobacterales
Burkholderiales
Bacillales
2.5 5.0 7.5 10.0
Count of isolates
D
MCI vs. WT
Enriched
NotSig
P = 0.05
−log10(adjusted P)
log2(Fold change)
Sorted by P value
Enterococcus faecium
Klebsiella oxytoca
Pseudomonas fortuita
Rothia kristinae
Bacillus amyloliquefaciens
Providencia stuartii
Rhodopseudomonas palustris
Klebsiella pneumoniae
E
P value 0.026 0.048 0.00021
Fecal ammonia content (ug/g)
WT Ef Ko Pf
F
P value 0.36 0.79 0.74
Blood ammonia (umol/mL)
WT Ef Ko Pf
G
Sum of Z-score
Pf
Ko
Ef
NOR
Ymaze
5 days of MWM test
Z-score
H
WT mice
week 0
Pf + FFA
week 2
Y-maze
NOR
MWM
week 4
Sacrifice
I
P = 0.038
Fecal ammonia content (ug/g)
Pf Pf+FFA
J
P = 0.036
Spontaneous alternation (%)
Pf Pf+FFA
K
P = 0.042
Recognition index (%)
Pf Pf+FFA
L
P = 0.16
Number of crossing island
Pf Pf+FFA
M
Time to find island (seconds)
Pf
Pf+FFA
P = 2x10⁻⁵
day1 day2 day3 day4
N
WT mice
week 0
uresea-BL21
week 2
Y-maze
NOR
MWM
week 4
Sacrifice
O
P = 0.026
Fecal ammonia content (ug/g)
vector urease
P
P = 0.021
Spontaneous alternation (%)
vector urease
Q
P = 0.03
Recognition index (%)
vector urease
R
P = 0.034
Number of crossing island
vector urease
S
AUC: P = 0.0032
Time to find island (seconds)
vector_BL21
urease_BL21
day1 day2 day3 day4


A
NH4Cl
week 0
NH4Cl-treated via drinking water
week 2
Y-maze
NOR
MWM
week 4
Sacrifice
B
P = 0.049
Fecal ammonia content (ug/g)
WT
NH4Cl
C
P = 0.35
Blood ammonia (umol/mL)
D
P = 2x10-4
Spontaneous alternation (%)
E
P = 0.0014
Recognition index (%)
J
Z-Score
MCI
NH4Cl
WT
Colon
Brain
F
Time to find island (seconds)
Experimental days
G
P = 0.023
Number of crossing island
H
Th17 cell differentiation
Brain: WT vs. NH4Cl
P = 0.012
NES = -1.47
Running Enrichment
Ranked List Metric
Rank in Ordered Dataset
I
TGF−beta signaling pathway
Colon: WT vs. NH4Cl
P = 0.039
NES = -1.44
Smad7
Jak2
K
0 2.5 3.0 3.5 NH4Cl (mM)
SMAD7
46 kDa
GAPDH
36 kDa
L
Transwell co-culture
SMAD7 overexpression
IMCC (Colonic Mucosal Epithelial Cells)
C8-D1A (Astrocytes)
M
1 2
JAK2
130 kDa
α-tubulin
50 kDa
1: Flag-Vector
2: Flag-SMAD7
N
WT NH4Cl WT MCI
JAK2
130 kDa
GAPDH
36 kDa
O
WT mice
week 0
5-FU i.p.
Construction of MCI model
week 2
AAV-SMAD7 / Vector (intrarectal administration)
week 4
Expression period
week 6
Y-maze / NOR / MWM
week 8
JAK2 expression
Sacrifice
Group
[MCI]: WT + 5-FU
[Vector]: MCI + AAV-Flag-Vector
[SMAD7]: MCI + AAV-Flag-SMAD7
P
MCI Vector SMAD7
SMAD7
46 kDa
GAPDH
36 kDa
JAK2
130 kDa
α-tubulin
50 kDa
Q
P = 0.011
P = 0.0055
Spontaneous alternation (%)
MCI
Vector
SMAD7
R
P = 0.0078
P = 0.0054
Recognition index (%)
S
Time to find island (seconds)
MCI
SMAD7
Vector
P = 0.048
Experimental days
T
P = 0.00062
P = 0.0059
Number of crossing island


A
Bacterial host contributing to urease
log10(abundance)
Lactobacillales
Bacillales
Clostridiales
Burkholderiales
Bifidobacteriales
Enterobacterales
Micromonosporales
Oceanospirillales
Micrococcales
Pseudomonadales
Planctomycetales
Salinisphaerales
Neisseriales
Propionibacteriales
Bacteroidales
Campylobacterales
Corynebacteriales
Rhizobiales
Streptomycetales
MCI
WT
B
KEGG Database
Keywords search "Substrate: NH3" "C00014: ammonia"
ammonia-metabolic gene list
Lactobacillales contributing to ammonia-metabolic gene
K00926
K00364
K01915
K01914
K01916
WT MCI
Abundance
C
P = 0.0018
log10(abundance of Lactobacillales)
WT
MCI
D
WT model
week 0
week 2
week 4
5-FU i.p.
L. mucosae oral gavage
Y-maze
NOR
MWM
Sacrifice
E
P = 0.34
Fecal ammonia content (ug/g)
MCI
Lm
F
P = 0.54
Spontaneous alternation (%)
WT
MCI+Lm
G
P = 0.33
Recognition index (%)
H
WT
MCI+Lm
Time to find island (seconds)
AUC: P = 0.064
Experimental days
I
P = 0.84
Number of crossing island
J
WT
MCI+Lm
SMAD7
46 kDa
GAPDH
36 kDa
JAK2
130 kDa
α-tubulin
50 kDa
K
WT mice
week 0
week 2
week 4
[MCI+Lm]
I. 5-FU i.p. + L. mucosae oral gavage
[MCI+HK-Lm]
II. 5-FU i.p. + Heat-killed L. mucosae oral gavage
[MCI+Lf]
III. 5-FU i.p. + L. fermentum oral gavage
Y-maze / Novel Object Recognition / Morris Water Maze
Sacrifice
L
P = 0.00071
P = 0.00243
P = 0.00089
Fecal ammonia content (ug/g)
MCI
MCI+Lm
MCI+HK-Lm
MCI+Lf
M
P = 2.5x10-7
P = 5.5x10-5
P = 1.2x10-6
Spontaneous alternation (%)
N
P = 0.0017
P = 0.0062
P = 0.0068
Recognition index (%)
O
MCI+HK-Lm
MCI+Lf
MCI+Lm
MCI
P = 0.049
P = 0.049
P = 0.0016
Time to find island (seconds)
Experimental days
P
P = 0.0344
P = 0.0082
P = 0.0062
Number of crossing island
Q
5xFAD mice
week 0
week 2
week 4
L. mucosae oral gavage
Y-maze
NOR
MWM
Sacrifice
R
P = 0.00788
Fecal ammonia content (ug/g)
WT
5xFAD
5xFAD+Lm
S
P = 2.6x10-6
Spontaneous alternation (%)
T
P = 0.0825
Recognition index (%)
U
P = 0.0137
5xFAD+Lm
5xFAD
WT
Time to find island (seconds)
Experimental days
V
P = 0.0316
Number of crossing island
W
WT
5XFAD
5XFAD+Lm
SMAD7
46 kDa
α-tubulin
50 kDa
JAK2
130 kDa
α-tubulin
50 kDa